Shape-Dependent Reducibility of Cuprous Oxide Nanocrystals

ARTICLE *in* THE JOURNAL OF PHYSICAL CHEMISTRY C · APRIL 2010

Impact Factor: 4.77 · DOI: 10.1021/jp101617z

Shape-Dependent Reducibility of Cuprous Oxide Nanocrystals

Huizhi Bao,[†,‡,§] Wenhua Zhang,[‡,∥] Daili Shang,[§] Qing Hua,[†,‡,§] Yunsheng Ma,[§] Zhiquan Jiang,[†] Jinlong Yang,*[,†,§] and Weixin Huang*[,†,‡,§]

Hefei National Laboratory for Physical Sciences at the Microscale, CAS Key Laboratory of Materials for Energy Conversion, Department of Chemical Physics, and Department of Materials Science and Engineering, University of Science and Technology of China, Hefei 230026, China

Received: February 23, 2010; Revised Manuscript Received: February 28, 2010

In this paper the reducibility of octahedral and cubic Cu_2O nanocrystals that respectively expose the (111) and (100) crystal planes has been investigated both experimentally and theoretically. Reduced either by H_2 or CO, the reduction temperature of octahedral Cu_2O nanocrystals is lower than that of cubic Cu_2O nanocrystals by more than 120 °C, which provides the unambiguous experimental results that the $Cu_2O(111)$ crystal plane is much more facile to be reduced than the $Cu_2O(100)$ crystal plane. The DFT calculation results reveal that the different reducibilities of octahedral and cubic Cu_2O nanocrystals arise from their different surface structures, in which the $Cu_2O(111)$ surface has coordination unsaturated Cu but the $Cu_2O(100)$ surface does not. The chemisorption and activation of CO and H_2 are stronger on the $Cu_2O(111)$ surface than on the $Cu_2O(100)$ surface. These results provide the convincing evidence for the shape-dependent surface reactivity of oxide nanocrystals.

1. Introduction

Engineering the surface of heterogeneous catalysts is critical to the design of new processes that minimize the number and amount of unwanted byproducts and that operate with high energy efficiency. Therefore, great efforts have been aimed at fundamentally understanding the surface structure−catalytic performance relationships and tuning the catalytic performance by controlling the surface structure of catalyst particles. The surface structure of a particle relies on the crystal planes that it exposes. In the past few decades, extensive surface science studies on bulk single crystals of metals and oxides under the ultrahigh vacuum conditions have identified that the variation in reactivity often depends on the exposed crystal plane.[1] However, technical catalysts are usually supported nanosized metal particles or metal oxide particles with poorly defined surface structure, which hampers the understanding of the surface structure−catalytic performance relationships and also may lead to the nonideal catalytic performance. The recent great advances in nanoscience enable the controllable synthesis of uniform nanocrystals with a well-defined shape that preferentially expose one type of crystal plane,[2] which can nicely serve as model systems for the fundamental investigations of the surface structure−catalytic performance relationship at the nanoscale and under "working" conditions and are also likely highly active and selective catalysts.[3] The shape-dependent catalytic performance has been reported for Pt,[4] Rh,[5] Ru,[6] Fe,[7] Ag[8] metal nanocrystals and CeO_2,[9] Co_3O_4[10] oxide nanocrystals.

Cuprous oxide (Cu_2O) has been used as a catalyst for several important oxidation reactions.[11] Uniform cubic and octahedral Cu_2O nanocrystals that respectively expose the (100) and (111) crystal plane have been successfully synthesized.[12] It has been reported that the octahedral Cu_2O nanocrystals show a higher activity in the photodegradation of rhodamine B and methylene blue molecules than the cubic Cu_2O nanocrystals.[13] In this paper, we report convincing experimental results of the shape-dependent reducibility of Cu_2O nanocrystals. Reduced either by H_2 or CO, octahedral Cu_2O nanocrystals are much more facile to be reduced than cubic Cu_2O nanocrystals. The accompanying DFT calculation results demonstrate that the different reducibilities of octahedral and cubic Cu_2O nanocrystals arise from their different surface structures. Since the reducibility of an oxide is closely related to its catalytic performance in oxidation reactions, our results infer that the catalytic activity of Cu_2O nanocrystals in oxidation reactions may depend on their shape and that octahedral Cu_2O nanocrystals are likely more efficient catalysts.

2. Experimental Section

The synthesis of Cu_2O nanocrystals followed Zhang et al.'s recipe.[12f] Typically, 5.0 mL of NaOH aqueous solution (2.0 $mol \cdot L^{-1}$) was added dropwise into 50 mL of $CuCl_2$ aqueous solution (0.01 $mol \cdot L^{-1}$) containing given amounts of poly(vinylpyrrolidone) (PVP, $M_W = 30\,000$) at 55 °C. After adequately stirring for 0.5 h, 5.0 mL of ascorbic acid aqueous solution (0.6 $mol \cdot L^{-1}$) was added dropwise into the solution. The mixed solution was adequately stirred for 3 h at 55 °C. The resulting precipitate was collected by centrifugation and decanting, followed by washing with distilled water and absolute ethanol, and finally dried in vacuum at RT for 12 h.

Powder X-ray diffraction (XRD) patterns were recorded on a Philips X'Pert PROS diffractometer using a nickel-filtered Cu Kα (wavelength: 0.154 18 nm) radiation source with the operation voltage and operation current being 40 kV and 50 mA, respectively. X-ray photoelectron spectroscopy (XPS) measurements were performed on an ESCALAB 250 high-performance electron spectrometer using monochromatized Al Kα ($h\nu = 1486.7$ eV) as the excitation source. The likely charging of samples was corrected by setting the binding energy

* To whom correspondence should be addressed. E-mail: huangwx@ustc.edu.cn (W.H.); jlyang@ustc.edu.cn (J.Y.).
† Hefei National Laboratory for Physical Sciences at the Microscale.
‡ CAS Key Laboratory of Materials for Energy Conversion.
§ Department of Chemical Physics.
∥ Department of Materials Science and Engineering.

10.1021/jp101617z
Published on Web 03/11/2010

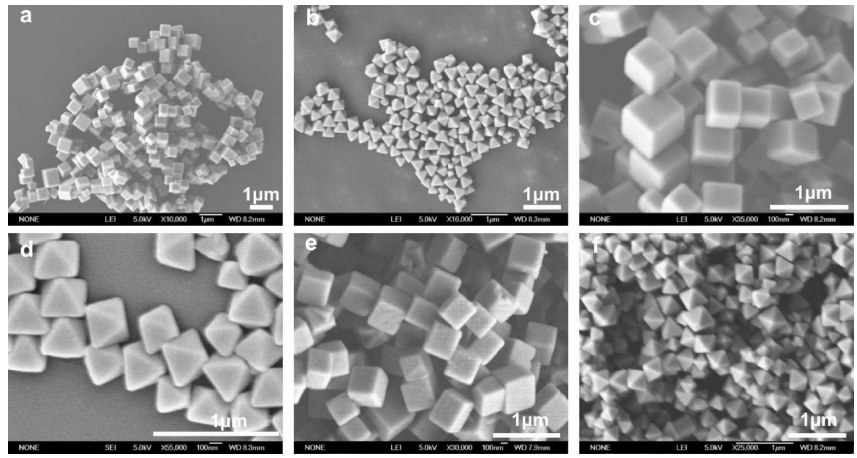

Figure 1. Representative SEM images of as-synthesized cubic (a and c) and octahedral (b and d) Cu_2O nanocrystals, cubic Cu_2O nanocrystals calcined in N_2 at 300 °C for 1 h (e), and octahedral Cu_2O nanocrystals calcined in N_2 at 200 °C for 1 h (f). The scale bar in all SEM images is 1 μm.

of the adventitious carbon (C 1s) to 284.5 eV. Scanning electron microscope (SEM) experiments were performed on a JEOL JSM-6700 field emission scanning electron microscope. Transmission electron microscopy (TEM) and selected area electron diffraction (ED) experiments were performed on a JEOL-2010 high-resolution transmission electron microscope. The reducibility of Cu_2O nanocrystals was investigated by the temperature-programmed reduction (TPR) technique employing H_2 (H_2-TPR) or CO (CO-TPR) as the reducing gas. Typically, 10 mg of catalyst was placed in a quartz reactor and heated at a rate of 5 °C/min. In H_2-TPR, 5% H_2 balanced with Ar with a flow rate of 20 mL/min was used and the consumption of H_2 was measured by a thermal conductivity detector (TCD). In CO-TPR, 1% CO balanced with Ar with a flow rate of 40 mL/min was used and the CO_2 product was online analyzed by a HIDEN QIC-20 gas analysis system. The reactivity of the adventitious carbon and likely organic compounds on the surface of Cu_2O nanocrystals was also studied by means of temperature-programmed reaction spectroscopy (TPRS) in which 10 mg of Cu_2O nanocrystals was heated in a quartz reactor in Ar (flow rate of 30 mL/min) at a heating rate of 5 °C/min and all likely products (CO_2, H_2O, H_2, CO, N_2, NH_3, NO, and NO_2) were online analyzed by a HIDEN QIC-20 gas analysis system.

3. Theoretical Calculation Methods

Theoretical calculations were performed within the spin-polarized density functional theory implemented in the DMol package.[14] The double-numeric quality basis set with polarization functions (DNP) was used. DFT semicore pseudopential (DSPP) and PBE functional[15] were used for all the atoms. A thermal smearing of 0.002 hartree and a real-space cutoff of 4.4 Å were adopted. In our calculations, the unpolarized $Cu_2O(111)$ was represented by four O−Cu−O layers with oxygen-terminated surfaces, and the polarized $Cu_2O(100)$ surface was represented by four O−Cu−O−Cu layers with one oxygen-terminated surface and another Cu-terminated surface in order to keep the stoichiometry ratio. The bottom two O−Cu−O or O−Cu−O−Cu layers were fixed at their bulk coordination. The vacuum space along the z direction was set as 18 Å, which was long enough to screen the interactions from image atoms. Our test calculations indicate that the k-points mesh with space of 0.06 $Å^{-1}$ was dense enough to give the converged energy. The adsorption of CO and H_2 was calculated on the relaxed oxygen-terminated surfaces.

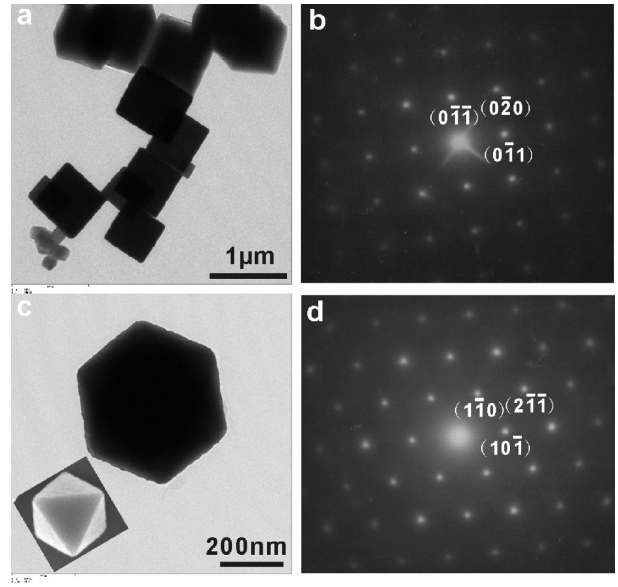

Figure 2. TEM images and corresponding electron diffraction patterns of as-synthesized cubic (a and b) and octahedral (c and d) Cu_2O nanocrystals. The inset shows the SEM image of one octahedral Cu_2O nanocrystal that corresponds to the TEM image.

4. Results and Discussion

Following Zhang et al.'s recipe,[12f] Cu_2O nanocrystals with a uniform cubic shape (Figure 1a and c) and those with a uniform octahedral shape (Figure 1b and d) were successfully synthesized with the molar ratio of PVP to $CuCl_2$ being 0 and 80, respectively. The cubic Cu_2O nanocrystals mostly have a size of 400−700 nm and the octahedral Cu_2O nanocrystals mostly have a size of ∼300 nm. The TEM images and corresponding ED patterns (Figure 2) clearly reveal that cubic and octahedral Cu_2O nanocrystals expose the (100) and (111) surfaces, respectively, agreeing with previous reports.[12] The powder XRD patterns of both octahedral and cubic nanocrystals (Figure 3A) can be well indexed to Cu_2O (JCPDS file number 78-2076). The XPS results (Figure 3B) show that the Cu $2p_{3/2}$ binding energy and the Cu LMM Auger peak kinetic energy of both samples are located at 932.2 and 916.2 eV, respectively, demonstrating that their surfaces remain Cu_2O.[16]

Interestingly, the reducibilities of octahedral and cubic Cu_2O nanocrystals differ significantly. Figure 4A shows the H_2-TPR

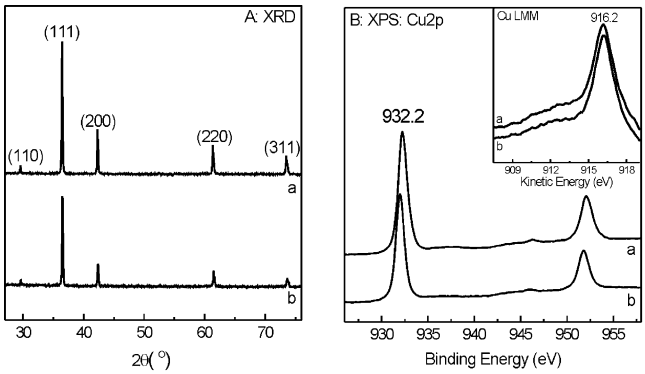

Figure 3. XRD (A) and Cu 2p XPS spectra (B) of as-synthesized cubic (a) and octahedral (b) Cu_2O nanocrystals. The inset shows the corresponding Cu LMM Auger peaks.

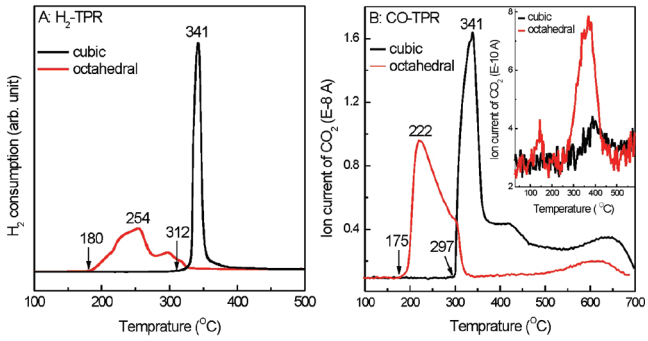

Figure 4. H_2-TPR (A) and CO-TPR (B) spectra of as-synthesized Cu_2O octahedral and cubic nanocrystals. The inset shows the CO_2-TPRS spectra of octahedral and cubic Cu_2O nanocrystals in Ar.

spectra in which the H_2 consumption peak corresponds to the reduction of Cu_2O by H_2 to produce H_2O. The cubic Cu_2O nanocrystals give a single reduction peak beginning at ~312 °C and reaching the maximum rate at 341 °C; however, the octahedral Cu_2O nanocrystals give multiple reduction peaks beginning at ~180 °C and reaching the maximum rate at 254 °C. The onset reduction temperature of octahedral Cu_2O nanocrystals is lower by 132 °C than that of cubic Cu_2O nanocrystals. The CO-TPR spectra (Figure 4B) in which the CO_2 peak corresponds to the reduction of Cu_2O by CO show the similar tendency. The reduction of cubic Cu_2O nanocrystals begins at ~297 °C and reaches the maximum rate at 341 °C, but the reduction of octahedral Cu_2O nanocrystals begins at ~175 °C and reaches the maximum rate at 222 °C, and the reduction temperature of octahedral Cu_2O nanocrystals is lower by 122 °C than that of cubic Cu_2O nanocrystals. The TPR results clearly demonstrate that Cu_2O octahedral nanocrystals are much more facile to be reduced either by H_2 or CO than Cu_2O cubic nanocrystals. The peak areas in the H_2-TPR and CO-TPR are similar for both octahedral and cubic Cu_2O nanocrystals, and their reduction reaction in CO and H_2 begins at the similar temperatures; however, the reduction reaction of Cu_2O in H_2 finishes before 400 °C, whereas that in CO extends to 700 °C. This indicates that there might be some differences between the reduction mechanism of Cu_2O by H_2 and that by CO, which needs further investigations.

The existence of adventitious carbon on the surface of particles is usually inevitable for the synthesis of powder samples. The XPS results show that the surface atomic concentration of adventitious carbon is 35% for cubic Cu_2O nanocrystals. Due to the use of PVP in the synthesis recipe, besides adventitious carbon, PVP was also detected on the

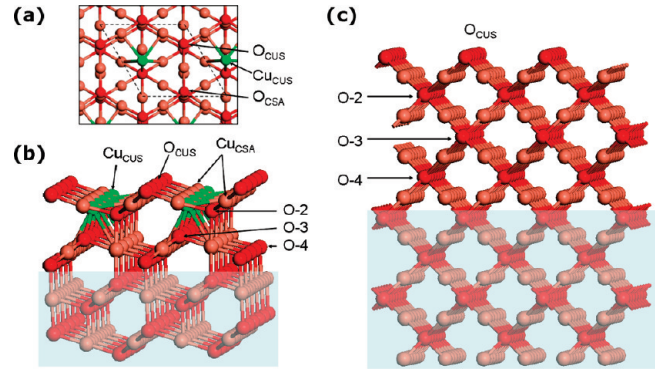

Figure 5. Optimized structures of $Cu_2O(111)$ and (100) surfaces: (a) top, (b) side view of $Cu_2O(111)$ surface, and (c) side view of $Cu_2O(100)$ surface. The shadow parts show the atoms fixed during the geometric optimization. The red, brick red, and green balls represent oxygen, coordinated saturated copper (Cu_{CSA}), and coordinated unsaturated copper (Cu_{Cus}) atoms, respectively.

surface of octahedral Cu_2O nanocrystals. The XPS results show that the surface atomic concentrations of carbon and nitrogen are 39% and 3.13% for octahedral Cu_2O nanocrystals, respectively. To check the influence of these surface carbon-containing species, we studied the reactivity of adventitious carbon and likely organic compounds on the surface of Cu_2O nanocrystals by means of TPRS in Ar. Only the formation of CO_2 was obviously observed (the inset in Figure 4B), and more CO_2 was produced from octahedral Cu_2O nanocrystals than from cubic Cu_2O nanocrystals, agreeing with the XPS results that the surface atomic concentration of adventitious carbon on octahedral Cu_2O nanocrystals is higher than that on cubic Cu_2O nanocrystals. However, the CO_2 peaks in the CO_2-TPRS spectra are weaker in intensity by 2 orders of magnitude than those in the CO-TPR spectra, implying that the adventitious carbon and likely organic compounds do not likely contribute to the significant difference between the reducibility of octahedral and cubic Cu_2O nanocrystals. We also found that the shapes and sizes of octahedral and cubic Cu_2O nanocrystals (Figure 1e and f) can be well preserved after calcination at high temperatures at 200 and 300 °C in N_2 for 1 h, respectively. This is reasonable because the melting point of Cu_2O crystals is 1232.0 °C. These observations demonstrate that the surface structures of octahedral and cubic Cu_2O nanocrystals do not likely change prior to the occurrence of reduction reaction. Therefore, the great difference between the reducibility of octahedral and cubic Cu_2O nanocrystals should arise from their different surface structures, i.e., different shapes.

The reduction of an oxide always initiates from the surface. The octahedral and cubic Cu_2O nanocrystals expose the (111) and (100) crystal planes, respectively. Therefore, our results demonstrate that the $Cu_2O(111)$ surface is much more facile to be reduced than the $Cu_2O(100)$ surface. DFT calculations were performed to understand the structures and reactivity of $Cu_2O(111)$ and $Cu_2O(100)$ surfaces. Figure 5 illustrates the optimized $Cu_2O(111)$ and $Cu_2O(100)$ surface structures. Both stable surfaces are O-terminated. On the $Cu_2O(111)$ surface, four types of atoms exist: coordinated unsaturated Cu (Cu_{CUS}) and O (O_{CUS}) and coordinated saturated Cu (Cu_{CSA}) and O (O_{CSA}). The distance between the nearest-neighboring Cu_{CUS} and O_{CSA} ($d(Cu_{CUS}-O_{CSA})$), the nearest-neighboring Cu_{CUS} and Cu_{CSA} ($d(Cu_{CUS}-Cu_{CSA})$), and the nearest-neighboring Cu_{CSA} and O_{CUS} ($d(Cu_{CSA}-O_{CUS})$) is 1.91, 2.51, and 1.83 Å, respectively; and the distance along the z direction between the nearest-neighboring Cu_{CSA} and Cu_{CUS} ($z(Cu_{CSA}-Cu_{CUS})$) is 0.23 Å. On

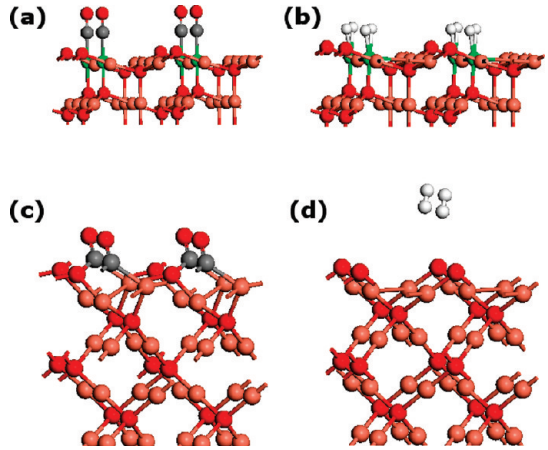

Figure 6. Most stable adsorption configurations for CO and H_2 adsorption on the $Cu_2O(111)$ and (100) surfaces: (a) CO on the $Cu_2O(111)$ surface; (b) H_2 on the $Cu_2O(111)$ surface; (c) CO on the $Cu_2O(100)$ surface; (d) H_2 on the $Cu_2O(100)$ surface. The red, brick red, green, gray, and white balls represent oxygen, Cu_{CSA}, Cu_{CUS}, carbon, and hydrogen atoms, respectively.

the $Cu_2O(100)$ surface, however, only three types of atoms exist: O_{CUS}, O_{CSA}, and Cu_{CSA}. The distance between the nearest-neighboring Cu_{CSA} and O_{CUS} ($d(Cu_{CSA}-O_{CUS})$) is 1.76 Å.

The chemisorptions of CO and H_2 on the $Cu_2O(111)$ and (100) surfaces were calculated, and Figure 6 illustrates the most stable configurations. On the $Cu_2O(111)$ surface, CO prefers to chemisorb on the Cu_{CUS} top site while it adsorbs on the $Cu_{CSA}-O_{CUS}$ bridge site of the $Cu_2O(100)$ surface. The adsorption energy of CO (1.52 eV) on the $Cu_2O(111)$ surface is larger than that (1.12 eV) on the $Cu_2O(100)$ surface. H_2 chemisorbs on the Cu_{CUS} top site of the $Cu_2O(111)$ surface but only physisorbs on the $Cu_2O(100)$ surface. The adsorption energy of H_2 (0.41 eV) on the $Cu_2O(111)$ surface is much larger than that (0.03 eV) on the $Cu_2O(100)$ surface, and the H−H bond length of H_2(ads) is 0.80 Å on the $Cu_2O(111)$ surface but 0.74 Å on the $Cu_2O(100)$ surface, suggesting that H_2 is highly activated upon the chemisorption on the $Cu_2O(111)$ surface. These results suggest that the $Cu_2O(111)$ surface is generally more active toward the chemisorption of reactants than the $Cu_2O(100)$ surface, which could be reasonably attributed to the existence of Cu_{CUS} on the $Cu_2O(111)$ surface. The chemisorption of CO and H_2 on the oxide surfaces is the first step in the reduction of oxide.[17] Therefore, although detailed DFT calculations are needed for a thorough understanding of the reduction behaviors of Cu_2O nanocrystals, it can be adequately concluded that the different surface structures of octahedral and cubic Cu_2O nanocrystals result in their different reducibilities.

The shape-dependent reducibility of Cu_2O nanocrystals is among the most unambiguous evidence for the shape-dependent reactivity of transitional metal oxides; moreover, its origin is successfully clarified at the molecular level. Zhou et al.[9a] reported that CeO_2 nanorods preferentially exposing (001) and (110) crystal planes are more active in CO oxidation than the irregular CeO_2 nanoparticles. Si and Flytzani-Stephanopoulos[9b] reported that the Au/CeO_2 catalyst with CeO_2 nanorods is much more active than that with CeO_2 nanocubes in the water−gas shift reaction. The catalytic activity of Co_3O_4 nanocrystals with different shapes was reported to follow the following order: nanosheets predominantly exposing the (112) crystal plane > nanobelts predominantly exposing the (011) crystal plane ≫ nanocubes predominantly exposing the (001) crystal plane.[10a] Xie et al.[10b] recently reported the excellent catalytic performance of Co_3O_4 nanorods predominantly exposing the (110) crystal plane with rich Co(III) in low-temperature CO oxidation. All these results vindicate the novel concept that the reactivity and catalytic activity of transitional metal oxides can be controlled and tuned by controlling their shape, which opens up a strategy for both the improvement of heterogeneous catalysts without the change of the catalyst composition and the design of highly efficient heterogeneous catalyst. We believe that the catalytic activity of Cu_2O nanocrystals in oxidation reactions is shape-dependent and that the octahedral Cu_2O nanocrystals are likely efficient catalysts, which are under investigation.

5. Conclusion

In summary, the octahedral Cu_2O nanocrystals exposing the (111) crystal plane are much more facile to be reduced either by H_2 or CO than the cubic Cu_2O nanocrystals exposing the (100) crystal plane. The different reducibilities of octahedral and cubic Cu_2O nanocrystals arise from their different surface structures, in which the $Cu_2O(111)$ surface has coordination unsaturated Cu but the $Cu_2O(100)$ surface does not. Therefore, the $Cu_2O(111)$ surface exhibits a higher activity toward the chemisorption and activation of CO and H_2 than the $Cu_2O(100)$ surface. These results provide the convincing evidence for the shape-dependent surface reactivity of oxide nanocrystals.

Acknowledgment. This work is financially supported by the National Science Foundation of China (20773113, 20973161), the Ministry of Science and Technology of China (2010CB923302), and the MPG-CAS partner group program.

References and Notes

(1) (a) Ertl, G. *Angew. Chem., Int. Ed.* **2008**, *47*, 3524. (b) Freund, H. J.; Pacchioni, G. *Chem. Soc. Rev.* **2008**, *37*, 2224.

(2) Burda, C.; Chen, X. B.; Narayanan, R.; El-Sayed, M. A. *Chem. Rev.* **2005**, *105*, 1025.

(3) (a) Bell, A. T. *Science* **2003**, *299*, 1688. (b) Somorjai, G. A.; Frei, H.; Park, J. Y. *J. Am. Chem. Soc.* **2009**, *131*, 16589. (c) van Bokhoven, J. A. *ChemCatChem* **2009**, *1*, 363.

(4) (a) Narayanan, R.; El-Sayed, M. A. *J. Am. Chem. Soc.* **2004**, *126*, 7419. (b) Tian, N.; Zhou, Z.-Y.; Sun, S.-G.; Ding, Y.; Wang, Z. L. *Science* **2007**, *316*, 732. (c) Bratlie, K. M.; Lee, H.; Komvopoulos, K.; Yang, P.; Somorjai, G. A. *Nano. Lett.* **2007**, *7*, 3097. (d) Lee, I.; Morales, R.; Albiter, M. A.; Zaera, F. *Proc. Natl. Acad. Sci. U.S.A.* **2008**, *105*, 15241. (e) Lee, I.; Delbecq, F.; Morales, R.; Albiter, M. A.; Zaera, F. *Nat. Mater.* **2009**, *8*, 132. (f) Komanicky, V.; Iddir, H.; Chang, K.-C.; Menzel, A.; Karapetrov, G.; Hennessy, D.; Zapol, P.; You, H. *J. Am. Chem. Soc.* **2009**, *131*, 5732. (g) Tsung, C. K.; Kuhn, J. N.; Huang, W.; Aliaga, C.; Hung, L.-I.; Somorjai, G. A.; Yang, P. *J. Am. Chem. Soc.* **2009**, *131*, 5816. (h) Schmidt, E.; Vargas, A.; Mallat, T.; Baiker, A. *J. Am. Chem. Soc.* **2009**, *131*, 12358.

(5) Zhang, Y.; Grass, M. E.; Kuhn, J. N.; Tao, F.; Habas, S. E.; Huang, W.; Yang, P.; Somorjai, G. A. *J. Am. Chem. Soc.* **2008**, *130*, 5868.

(6) Karim, A. M.; Prasad, V.; Mpourmpakis, G.; Lonergan, W. W.; Frenkel, A. I.; Chen, J. G.; Vlachos, D. G. *J. Am. Chem. Soc.* **2009**, *131*, 12230.

(7) Chen, Y.-X.; Chen, S.-P.; Zhou, Z.-Y.; Tian, N.; Jiang, Y.-X.; Sun, S.-G.; Ding, Y.; Wang, Z. L. *J. Am. Chem. Soc.* **2009**, *131*, 10860.

(8) Xu, R.; Wang, D.; Zhang, J.; Li, Y. *Chem. Asian J.* **2006**, *1*, 888.

(9) (a) Zhou, K.; Wang, X.; Sun, X.; Peng, Q.; Li, Y. *J. Catal.* **2005**, *229*, 206. (b) Si, R.; Flytzani-Stephanopoulos, M. *Angew. Chem., Int. Ed.* **2008**, *47*, 2884.

(10) (a) Hu, L.; Peng, Q.; Li, Y. *J. Am. Chem. Soc.* **2008**, *130*, 16136. (b) Xie, X. W.; Li, Y.; Liu, Z. Q.; Haruta, M.; Shen, W. J. *Nature* **2009**, *458*, 746.

(11) (a) Jones, P. M.; May, J. A.; Brad Reitz, J.; Solomon, E. I. *J. Am. Chem. Soc.* **1998**, *120*, 1506. (b) Nagase, K.; Zheng, Y.; Kodama, Y.; Kakuta, J. *J. Catal.* **1999**, *187*, 123. (c) White, B.; Yin, M.; Hall, A.; Le, D.; Stolbov, S.; Rahman, T.; Turro, N.; O'Brien, S. *Nano. Lett.* **2006**, *6*, 2095.

(12) (a) Gou, L.; Murphy, C. J. *Nano. Lett.* **2003**, *3*, 231. (b) Siegfried, M. J.; Choi, K.-S. *Angew. Chem., Int. Ed.* **2005**, *44*, 3218. (c) Li, H.; Liu, R.; Zhao, R.; Zheng, Y.; Chen, W.; Xu, Z. *Cryst. Growth Des.* **2006**, *6*, 2705. (d) Siegfried, M. J.; Choi, K.-S. *J. Am. Chem. Soc.* **2006**, *128*, 10356. (e) Kuo, C.-H.; Chen, C.-H.; Huang, M. H. *Adv. Funct. Mater.* **2007**, *17*,

3773. (f) Dong, D.-F.; Zhang, H.; Guo, L.; Zheng, K.; Han, X.-D.; Zhang, Z. *J. Mater. Chem.* **2009**, *19*, 5220.

(13) (a) Kuo, C.-H.; Huang, M. H. *J. Phys. Chem. C* **2008**, *112*, 18355. (b) Ho, J.-Y.; Huang, M. H. *J. Phys. Chem. C* **2009**, *113*, 14159.

(14) (a) Delly, B. *J. Chem. Phys.* **1990**, *92*, 508. (b) Delly, B. *J. Chem. Phys.* **2000**, *113*, 7756. (c) Soon, A.; Söhnel, T.; Idriss, H. *Surf. Sci.* **2005**, *579*, 131.

(15) Perdew, J. P.; Burke, K.; Ernzerhof, M. *Phys. Rev. Lett.* **1996**, *77*, 3865.

(16) Moulder, J. F.; Stickle, W. F.; Sobol, P. E.; Bomben, K. D. *Handbook of X-ray Photoelectron Spectroscopy*; Perkin-Elmer Corporation: Eden Prarie, MN, 1992.

(17) (a) Rodriguez, J. A.; Hanson, J. C.; Frenkel, A. I.; Kim, J. Y.; Pérez, M. *J. Am. Chem. Soc.* **2002**, *124*, 346. (b) Kim, J. Y.; Rodriguez, J. A.; Hanson, J. C.; Frenkel, A. I.; Lee, P. L. *J. Am. Chem. Soc.* **2003**, *125*, 10684.

JP101617Z